Analyst

PAPER

View Article Online
View Journal | View Issue

Cite this: *Analyst*, 2014, **139**, 1913

Ion dynamics in a trapped ion mobility spectrometer†

Diana Rosa Hernandez,[a] John Daniel DeBord,[a] Mark E. Ridgeway,[b] Desmond A. Kaplan,[b] Melvin A. Park[b] and Francisco Fernandez-Lima*[a]

Received 22nd November 2013
Accepted 17th January 2014

DOI: 10.1039/c3an02174b

www.rsc.org/analyst

In the present paper, theoretical simulations and experimental observations are used to describe the ion dynamics in a trapped ion mobility spectrometer. In particular, the ion motion, ion transmission and mobility separation are discussed as a function of the bath gas velocity, radial confinement, analysis time and speed. Mobility analysis and calibration procedure are reported for the case of sphere-like molecules for positive and negative ion modes. Results showed that a maximal mobility resolution can be achieved by optimizing the gas velocity, radial confinement (RF amplitude) and ramp speed (voltage range and ramp time). The mobility resolution scales with the electric field and gas velocity and $R = 100–250$ can be routinely obtained at room temperature.

Introduction

Ion Mobility Spectrometry (IMS) has been widely used in the detection of chemical warfare agents, illicit drugs, explosives, and more recently in the separation and detection of biomolecules.[1–9] Developed in the late 1970s, IMS permits the separation of ions in the gas-phase by their size-to-charge ratio (Ω/z) in the presence of a neutral gas. Initially known as plasma chromatography or ion chromatography, IMS has been coupled to mass spectrometry (MS) to obtain fast, complementary separations (*i.e.*, Ω/z and m/z).[10–13] In particular, IMS-MS offers several advantages over traditional MS, including separation of ions from mixtures based on the composition and charge state, the ability to separate geometric isomers, increase the dynamic range and discrimination against chemical noise.[14–19]

A variety of forms and designs of IMS analysers have been described in the literature.[20] A leading force behind these efforts has been the drive for higher mobility separation and higher ion transmission. For example, variants of the basic, high-pressure drift tube incorporated entrance and exit ion funnels to increase ion transmission, thus turning the basic drift tube into a powerful analyzer.[21] In a different approach, ion transmission has also been increased by using periodic-focusing DC ion guides.[22,23] Other techniques have been used to add a degree of separation prior to MS analyses (*e.g.*, field asymmetric IMS,[24] differential mobility spectrometer,[3,4,25] segmented quadrupole drift cell,[26] cylindrical drift tubes,[27] and transient wave ion guide[28]). Several research groups have focused on achieving high resolution IMS separation ($R > 50$) as this factor mainly limits the information that can be experimentally derived.[29–32] We have recently introduced a Trapped Ion Mobility Spectrometer (TIMS) that can be easily integrated into a mass spectrometer (MS) for IMS-MS analyses and which is capable of producing high resolution IMS separations.[33,34] The most significant breakthrough of TIMS technology lies in the fact that mobility separation can be tuned from low to high according to the analytical challenge. However, a detailed understanding of the ion dynamics in a TIMS cell, modes of operation, performance and limitations is necessary for the development of analytical applications.

In the present paper, a detailed description of the ion dynamics inside a Trapped Ion Mobility Spectrometer (TIMS) is discussed. In particular, the influence of the electrode geometry, bath gas flow, radial trapping potential, and ramp speed on the mobility resolution is modeled theoretically and compared with experimental values. The methodology to determine an accurate collision cross-section from TIMS measurements is also provided.

Experimental

TIMS analyzer

A TIMS cell consists of three main sections: entrance funnel, analyzer section and exit funnel (shown in the cross-section in Fig. 1). Ions are typically generated using an Electrospray Ion Source (Apollo II design, Bruker Daltonics Inc., MA) and introduced into the TIMS device *via* a glass ion transfer capillary. The TIMS sections are constructed from a set of segmented ring electrodes supported on PC boards (plate thickness of 1.6 mm).

[a]*Department of Chemistry and Biochemistry, Florida International University, Miami, USA. E-mail: fernandf@fiu.edu; Fax: +1 305 348 3772; Tel: +1 305 348 2037*

[b]*Bruker Daltonics, Inc., Billerica, Massachusetts 01821, USA*

† Electronic supplementary information (ESI) available: Detailed information on the structure of the sphere-like molecules considered here. In addition, ion trajectory simulations and mobility resolution dependence on the gas velocity are shown. See DOI: 10.1039/c3an02174b

Each electrode is composed of four electrically isolated segments (two shown in the cross-section in Fig. 1 for each PC board). The basic design of the electrodes is the same throughout the three sections – only the inner diameter is varied from 26 to 8 mm and from 8 to 1 mm in the entrance and exit funnels, while kept constant at 8 mm in the analyzer section. In the entrance and exit funnel sections, the plates are spaced 1.5 mm from each other. However, in the analyzer section, plates are separated by an insulating gasket material (kapton, 0.125 mm thickness) which forms a gas tight seal. The length of the entrance funnel, analyzer section and exit funnel are 50, 46 and 15 mm, respectively. The segmented plate design has the advantage that it can be used to form a dipolar field, as is typical in ion funnels, or a quadrupolar field.[35] In the entrance and exit funnel sections, the RF potential applied to the ion funnel is 180° out of phase between adjacent plates. This results in a pseudo-potential, which simply keeps the ions away from the funnel walls. The same RF waveform is used throughout the TIMS funnel. However, in the analyzer section, the phase of the RF potential does not alternate between adjacent plates but only between adjacent segments. Importantly, the purpose of the quadrupolar field in the analyzer section is to confine (trap) the ions radially and avoid ion losses due to diffusion.

The gas flow velocity in the analyzer region is regulated by the pressure difference between the entrance funnel (P_1) and exit funnel (P_2) regions. In practice, the pressure difference is regulated by changing the pumping impedance using a butterfly valve. The operating pressure difference (few mbar) produces a cylindrically symmetric gas flow. Mobility separation in a TIMS device can be performed using different gases or mixtures in accordance with the analytical problem to be solved. In the examples presented herein, the separation was performed using nitrogen as the bath gas at *ca.* 300 K with typical entrance funnel and exit funnel pressures of $P_1 = 1.0$–2.6 and $P_2 = 1.0$ mbar, respectively.

TIMS-MS operation sequence

The TIMS funnel can be operated in "transmission" mode or "IMS" mode. In transmission mode, the DC potentials on all the funnel elements are set to continually push ions downstream – *i.e.* without a mobility separation. In practice, the analyzer entrance potential is set higher – *i.e.* more repulsive to the ions – than that of the analyzer exit. Similarly, the funnel entrance and deflection plate are set to successively higher potentials when operating in transmission mode. In transmission mode the instrument produces conventional mass spectra.

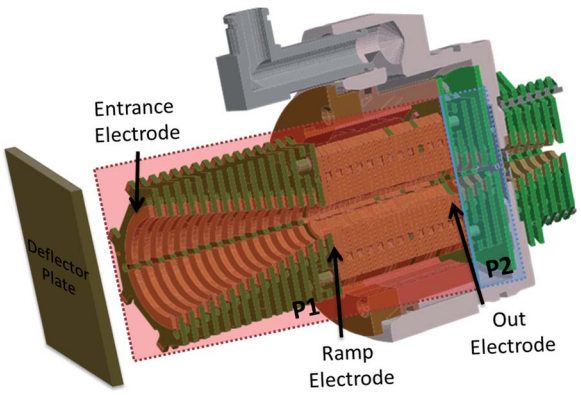

Fig. 1 Cross-sectional view of the TIMS entrance funnel, analyser section and exit funnel.

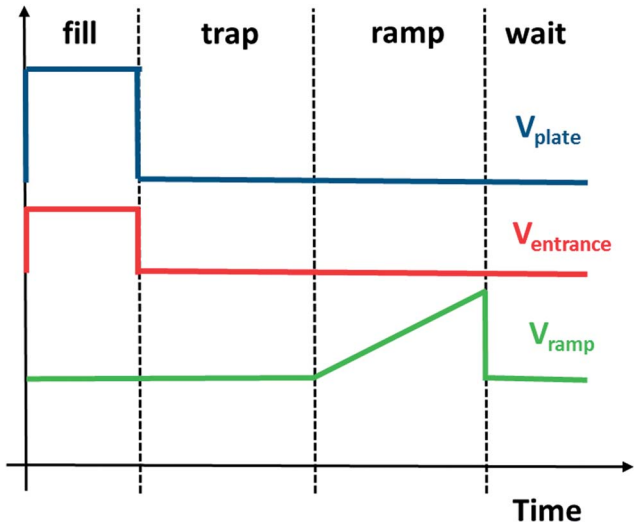

Fig. 2 Time sequence of a mobility analysis in a TIMS analyser for positive ion mode. Notice that fill and trap times can be adjusted for the maximum mobility resolution and sensitivity and for kinetic measurements, respectively.

In IMS mode, the sequence begins with ion loading of the analyzer section (Fig. 2). The DC potentials on the deflection plate, funnel entrance, and analyzer entrance are set to push ions orthogonally out of the gas stream from the capillary, through the entrance funnel, and into the analyzer section. However, the DC potential on the analyzer entrance is set below that of the exit so as to produce a retarding field. The gas flow – from left to right in Fig. 1 – pushes the ions downstream with a "force" in accordance with the ions' mobility. Ions within a given mobility range thus become trapped by the DC electric field which prevents the ions from progressing downstream, while the gas flow prevents the ions from returning upstream, and the RF quadrupolar pseudo-potential which prevents the ions from escaping radially. In practice, the potential profiles are produced by a network of precision resistors operating as a voltage divider. Thus, to produce the given potential profiles, voltages are applied to the deflection plate, capillary exit, funnel entrance, analyzer entrance, and analyzer exit. With these few inputs to the resistor network, the complete potential profile is defined. At all times, the axial electric field is kept under the low field limit (E/p < 10 V cm^{-1} torr^{-1}) throughout the TIMS device.[36,37]

The filling time can be tuned according to the number of ions (ESI beam current) coming from the capillary, with a typical filling time of about 10 ms. Ions trapped in the analyzer section will assume positions (or electrode number) depending on their mobilities. The DC electric field strength, E_x, is

dependent on the position – highest field strength nearer the exit end. Thus, the lowest mobility ions come to a "stop" in the highest field strength region (nearer the exit end of the analyzer section) whereas the highest mobility ions assume positions in the lowest field strength region (nearer the analyzer entrance). Following the trapping period, additional ions are prevented from entering the analyzer section by lowering the potential on the deflection plate – *i.e.* by making the deflection plate potential attractive. When the deflection plate potential is attractive, ions exiting the capillary are accelerated towards the deflection plate. Trapped ions in the analyzer section, however, are unperturbed by the deflection plate potential variation. Mobility analysis of the trapped ions consists of reducing the strength of the retarding electric field in the analyzer section stepwise over time.

To reduce the retarding field strength in the analyzer section, the potential at the analyzer entrance is increased at a constant rate – *i.e.* "scanned" – from its initial value to an end value – in this case, the analyzer exit potential. As the field strength is reduced, the trapped ions shift to new positions in the analyzer – with ions of a given mobility always residing at a position having a given field strength. As the retarding field strength is reduced, ions of successively higher mobilities are pushed by the gas flow out of the analyzer region. Ions exiting the analyzer section are focused by the exit funnel towards the entrance ion optics of a mass spectrometer. In particular, for the examples shown here, a maXis Impact Q-UHR-ToF (Bruker Daltonics Inc., MA) was coupled to the TIMS analyzer. The measured ion current plotted over the course of the voltage ramp (*i.e.*, ramp speed = voltage/ramp time) provides the ion mobility spectrum from low ion mobilities to high ion mobilities.

TIMS time sequences and voltages were controlled using the in-house software, written in National Instruments Lab VIEW, and synchronized with the MS acquisition program. In particular, voltages were defined using National Instruments cards (NI-PXI-6704, NI-PXI-6289, NI-PXI-6361) and a 1 GHz digitizer (NI-PXI-5154) was used for the MS data acquisition. All cards were housed in a 1073e PXI chassis, operated by a computer PXIe extension bus. The TIMS-MS experiment was synchronized with the TOF start (extraction trigger). The digitizer trigger was internally routed through the PXI chassis and sent to the PXI-6361. A digital pattern was then output at a rate of 10 MHz, which was triggered by the routed digitizer trigger. The digital pattern, defined by the user, consisted of three TTL triggers which were used for: (1) trapping ions in the analyzer section, (2) blocking ions from entering the analyzer section, and (3) signaling the start of the voltage ramp in the analyzer section for ion elution. The ramp voltage was controlled by the PXI-6289 analog output (AO). The ramp voltage range (V_{ramp}) and time (T_{ramp}) were defined in the software and built as an array of output voltages. The output voltage of the PXI-6289 ($\pm$ 10 V AO) was amplified using an in-house 15$\times$ amplifier capable of 50 kHz ramp rates. The internally routed trigger was also used as the output clock of the PXI-6289, which results in the TIMS voltage steps synchronized with the TOF pulses. MS data were acquired from the digitizer for each ramp step (*i.e.*, 1 record set at a time). After a full set of TIMS records were acquired from the digitizer, all of the PXI cards were reset and the next TOF trigger restarted the process again. This acquisition process (*i.e.*, re-initializing the cards) was required due to the slow data transfer rate from the digitizer to the computer and to ensure proper timing synchronization during the entire TIMS-MS experiment.

Materials and reagents

Molecules used in this study were purchased from Sigma (St. Louis, MO) and used as received. Samples were electro-sprayed at a concentration of 1–10 μmolar in a 1 : 1 (v/v) water–methanol solution. An ESI Tuning Mix calibration standard (Tunemix, G2421A) was purchased from Agilent Technologies (Santa Clara, CA) and used as received.[38] Details of the ESI tuning mix calibration structures can be found in the ESI.†

Theoretical

Ion and gas dynamics in a TIMS cell

To better understand the effect of the bath gas flow on the TIMS performance and operation, the pressure gradient in the TIMS cell was modelled (Fig. 3). A cylindrical geometry was used and the mass flow and energy equations were solved simultaneously for the case of nitrogen as the bath gas and using the P_1 and P_2 pressure values as boundary conditions for the calculations. The Fluent 6.2.16 (Fluent Inc., Lebanon, NH) software was used.[39]

Inspection of Fig. 3 shows that the velocity profile is near homogenous in the central region (tens of m s^{-1} for the pressure studied) and that the gas velocity decreases in magnitude near the wall of the analyser region. The end result is a parabolic profile as a consequence of the friction of the gas molecules near the walls. This parabolic flow profile determines the trapping conditions during TIMS operation; that is, in a TIMS device the basis for the mobility separation lies in compensation of the drag force (proportional to the gas velocity) with the electric force (increasing in magnitude from left to right with the electrode positions). Inhomogeneities in the gas profile could also influence the ion transfer in funnel 2 but at this stage the gas velocity is much lower and has a smaller effect.

To have a better understanding of the correlation between the gas velocity and the ion trajectories, the ion dynamics inside the TIMS cell were studied using an in-house routine incorporated into a Simion 3D (ref. 40) user developed program. In the ion simulations, an Elastic Hard Sphere Scattering model (EHSS) for the ion-neutral collisions was used.[41] The bath gas temperature and velocity, electric field gradient, RF amplitude and frequency, and collision cross-sections were used as simulation input parameters.

Two cases were compared with the experimental observation in order to evaluate the bath gas velocity parabolic profile (see Fig. 4): one dimensional (v_x) and three dimensional profiles (v_{xyz} parabolic). At low RF amplitude values, ions are poorly confined and diffuse toward the TIMS analyser walls and are neutralized. However, as the RF amplitude increases, ions are confined

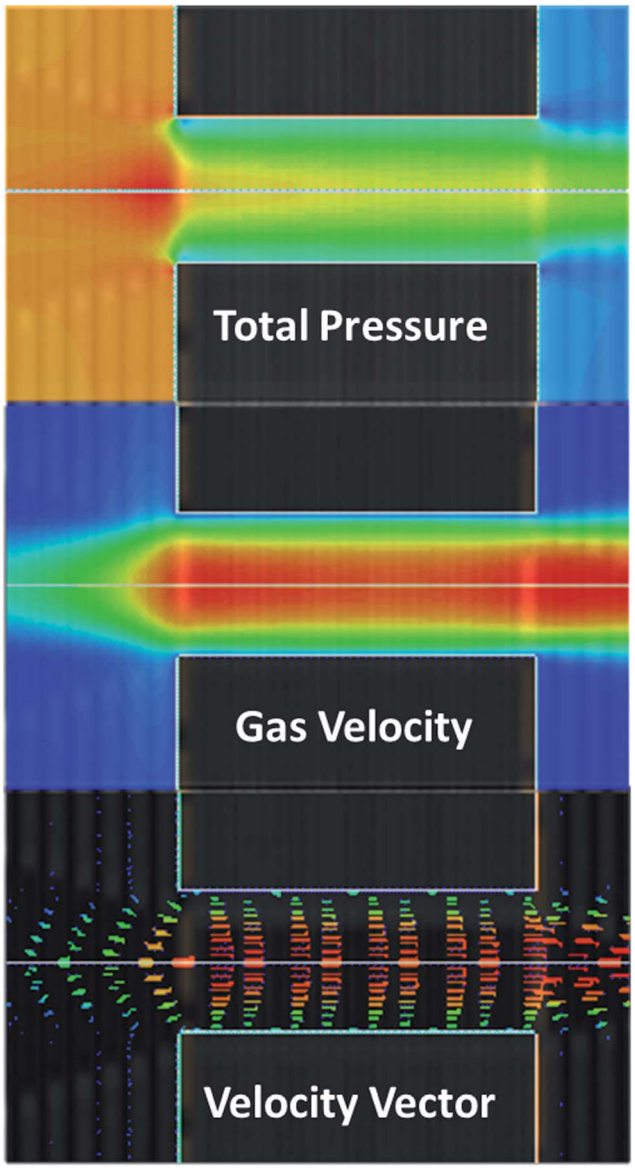

Fig. 3 Total pressure, gas velocity and velocity vector profiles for nitrogen in the TIMS analyser section. P_1 and P_2 were used as boundary conditions ($P_1 = 2.6$ and $P_2 = 1.0$ mbar). Scale: red: high and blue low.

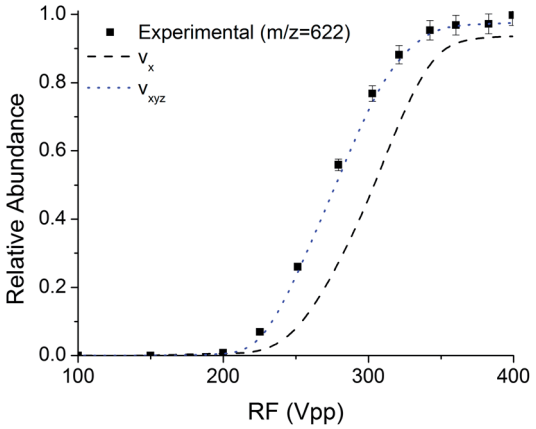

Fig. 4 Comparison of the experimental and theoretical relative ion abundance (m/z = 622) as a function RF amplitude. Theoretical simulations were performed using one (v_x = 70 m s^{-1}) and three (v_{xyz}, parabolic) dimensional gas profiles for the same conditions as shown in Fig. 3.

towards the center of the TIMS analyser and higher ion abundances are observed. Comparison between the simulations shows that a better agreement is obtained when a three dimensional profile is used compared to a one-dimensional profile. In particular, this effect is more pronounced at lower RF amplitudes, where the ion cloud is more spread in the radial direction and a larger gas velocity gradient is experienced by the ions trapped in the cylindrical TIMS analyzer section.

Similar conclusions can be obtained from the inspection of the ion clouds as a function of the RF amplitude in the TIMS analyzer section (Fig. 5). When no RF is applied, ions are confined in the axial direction by the electric and drag forces. In the radial direction, ions will diffuse over time and the ion population will decrease as they get neutralized by collisions with the walls. With the increase of the radial force (or RF amplitude), the ion cloud is pushed towards the center and ion confinement occurs.

The size of the ion cloud is defined by the radial and axial confinement and by the number of ions (charges) that are confined. If the radial confinement is too high, ions will spread in the axial direction to compensate for the coulombic repulsion of the ion cloud counterparts. That is, the higher the number of ions and the higher the RF amplitude the larger the axial spread of the ion cloud. Similar effects related to the number of ions trapped have been observed in other trapping devices (*e.g.*, Paul trap, linear ion trap, ICR cell, *etc.*).[42–46] In TIMS, the presence of the bath gas (higher pressures compared to other trapping devices, few mbar) induces larger changes on the ion trajectories by the ion-neutral collisions, ion-neutral collision being the defining parameter of the ion motion. Analogous to drift tube experiments, reduction of the bath gas temperature will reduce the ion diffusion and increase the mobility resolution (see the example in the ESI† for bath gas at *ca.* 80 K). Nevertheless, there are practical challenges associated with the use of lower bath gas temperatures due to the high gas flow used in the TIMS analyzer.

TIMS separation

The theoretical concept behind TIMS is the use of an electric field to hold ions in place against a moving gas. The TIMS operation is analogous to that of parallel flow ion mobility analyzers,[47,48] with the main difference that ions are also confined radially to guarantee higher transmission and sensitivity. In particular, the separation in a TIMS device can be described in the center of mass frame using the same principles as in a conventional drift tube.[49,50] That is, in conventional drift cells ions are pushed through a stationary gas whereas in the TIMS analyzer ions are held in place against a moving gas. Since mobility separation is related to the number of ion-neutral collisions (or drift time in traditional cells), the mobility separation in a TIMS device depends on the bath gas drift velocity,

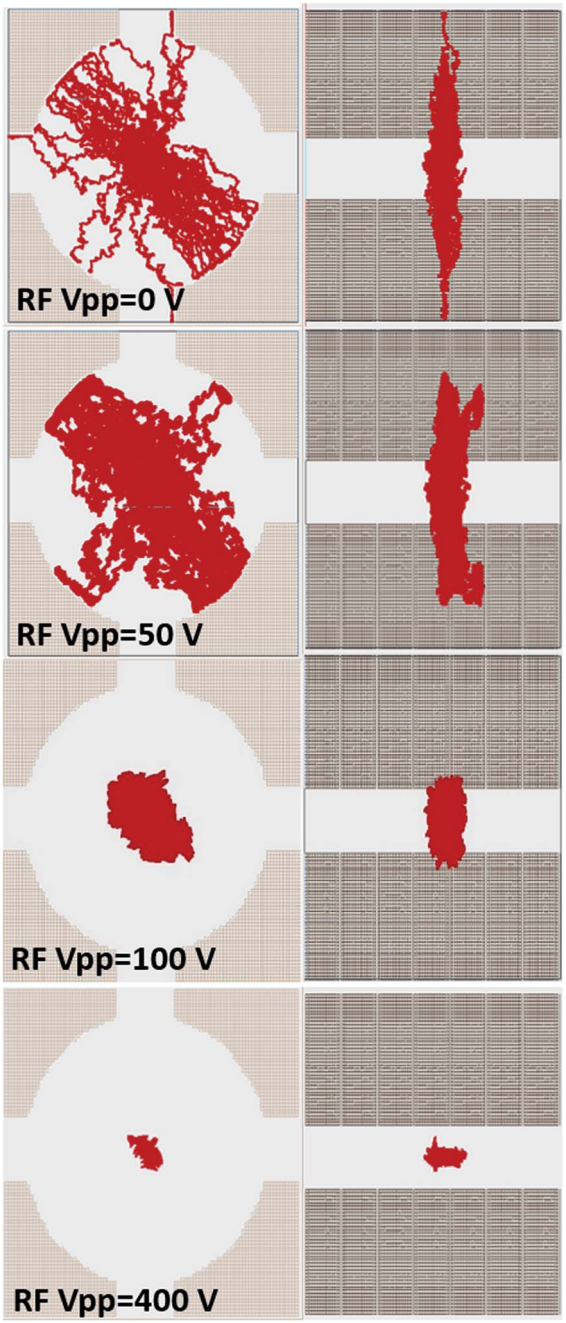

Fig. 5 Ion trajectories as a function the RF amplitude theoretical relative on abundance ($m/z = 622$) as a function RF in the TIMS analyser. Simulations were performed at the same conditions as Fig. 3 and 4 for $m/z = 322$ and using an RF frequency of 890 kHz.

ion confinement and ion elution parameters. For example, the mobility range (K_a–K_b) of an analysis is directly related to the ratio of the gas velocity (v_g) and the axial electric field range (E_a–E_b). The mobility of a given ion (i) can be extracted from the electric field (E_x(i)) at which the ion package elutes. In practice, this can be related to the elution voltage (V_{elut}(i)) at which this process occurs relative to the voltage applied to the last electrode (V_{out}) of the mobility section:

$$K_i = v_g/E_x(i) = A(1/(V_{out} - V_{elut}(i)) \quad (1)$$

where A is a calibration constant that can be experimentally determined using known standards, either internally or externally. That is, the elution voltage is a characteristic parameter of the ion mobility for the same bath gas and velocity and can be calculated from the total IMS time using eqn (2) (see Fig. 6).

The elution voltage is independent of the voltage ramp characteristics; however, the width of the elution voltage peak changes with the strength of the radial confinement (this is ultimately related to the mobility resolution as discussed later). For example, with the increase of the radial field (RF amplitude) an increase in the elution voltage FWHM is observed. We attribute this increase to the spread of the ion cloud in the axial dimension, in good agreement with the simulations shown in Fig. 5. Noticed that the axial spread is limited by the width of the electric field (ΔE) necessary to trap the ion cloud; that is, the elution voltage has a limited peak width. This trend can be observed for the case of $m/z = 622$ in Fig. 6. Different ion clouds (*e.g.*, mass, charge and size) will respond differently to the RF radial confinement. That is, since larger molecules (assuming +1 charge for simplicity) will require a higher RF amplitude to be trapped, the axial spread will be observed at larger RF amplitudes. If the radial spread is large (close to ΔE limit), the ion-neutral collision (or diffusion) will lead to a decrease in the ion population. At the same time, this condition will impose a higher limit on the elution voltage FWHM, and consequently a lower limit in the mobility resolution.

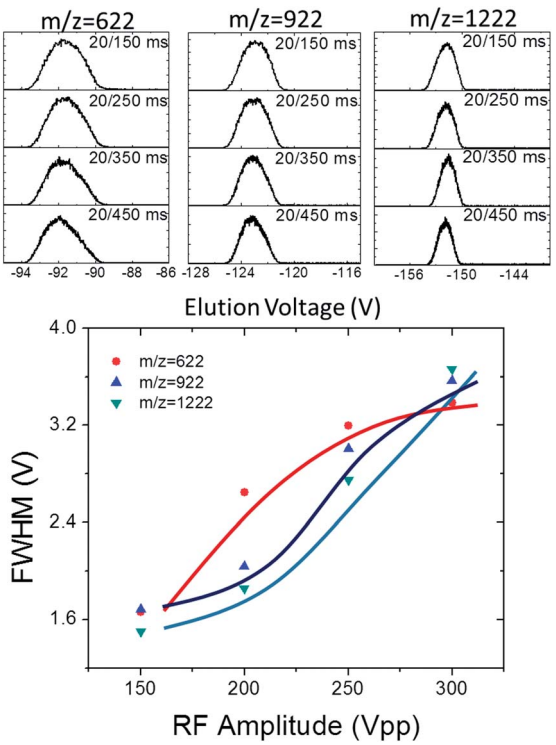

Fig. 6 (Top) Elution voltage (V_{elut}) dependence on the fill/ramp time (20/150–20/450 ms) for $m/z = 622$, 922 and 1222 at RF 250 V_{pp}. (Bottom) Dependence of the elution voltage peak width (FWHM) as a function of RF amplitude.

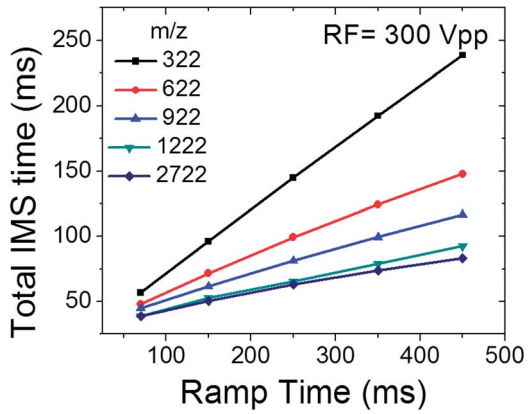

Fig. 7 Dependence of the total IMS time on the ramp time as a function of *m*/*z*.

Mobility calibration

In a TIMS device, the total analysis time can be described as:

$$\begin{aligned}\text{Total IMS time} &= T_{\text{trap}} + (V_{\text{elut}}/V_{\text{ramp}})T_{\text{ramp}} + \text{ToF} \\ &= T_{\text{o}} + (V_{\text{elut}}/V_{\text{ramp}})T_{\text{ramp}}\end{aligned} \quad (2)$$

where, T_{trap} is the thermalization/trapping time, ToF is the time after the mobility separation, and V_{ramp} and T_{ramp} are the voltage range and time required to vary the electric field, respectively. The elution voltage can be experimentally determined by varying the ramp time for a constant ramp voltage. This procedure also determines the time ions spend outside the separation region T_{o} (*e.g.*, ion trapping and time-of-flight). Experimental results show the linear dependence of the total IMS time with the ramp time for all *m*/*z*'s studied (see the example in Fig. 7).

From the slope and the intercept of this graph the mobility values can be determined if the calibration constant *A* is known (see eqn (1) and (2)). The mobility and collision cross-section values presented in Table 1 were obtained by calculating the calibration constant from mobility measurements performed in traditional drift tube IMS using the same nitrogen bath gas and temperature (*ca.* 300 K). For the case of negative ion values reported in Table 1, the same calibration constant *A* was considered. Notice that the procedure described here provides accurate mobility measurements from first principles. Mobility values (K) were correlated with CCS (Ω) using the equation:

$$\Omega = \frac{(18\pi)^{1/2}}{16}\frac{z}{(k_{\text{B}}T)^{1/2}}\left[\frac{1}{m_{\text{I}}}+\frac{1}{m_{\text{b}}}\right]^{1/2}\frac{1}{K}\frac{760}{P}\frac{T}{273.15}\frac{1}{N^*} \quad (3)$$

where z is the charge of the ion, k_{B} is the Boltzmann constant, N^* is the number density and m_{I} and m_{b} refer to the masses of the molecular ion and bath gas molecule, respectively.

Mobility resolution

The mobility resolution in a TIMS device is defined by:

$$R = K/\Delta K = (V_{\text{out}} - V_{\text{elut}})/\Delta V_{\text{elut}} \quad (4)$$

In a traditional drift tube, the resolution is defined by the device length, bath gas pressure and temperature and the applied electric field.[51,52] In a TIMS device, different mobilities are trapped at different electric field strengths for the same velocity of the gas, and hence different mobility resolutions will be observed. In addition, as noticed in previous results, the radial confinement may change the elution voltage FWHM (axial spread of the ion cloud).

In a TIMS device, as a general rule the resolution mainly depends on three parameters: (a) the bath gas velocity, (b) the electric field ramp speed ($\Delta V_{\text{ramp}}/T_{\text{ramp}}$) and (c) the RF confinement. In the case of the bath gas velocity, an increase in the bath gas velocity requires an increase in the electric field to

Table 1 Mobility values of the ESI Tune Mix calibration standard. Negative values were obtained using the calibration constant *A* obtained from positive ion values

Monoisotopic mass	Formula	K_{o} [cm^2 V^{-1} s^{-1}]	CCS [Å^2]
118.086255	$C_2H_3NO_2(CH_3)_3[M]^{+1}$	1.920	116.2
322.048121	$P_3N_3(OCH_3)_6[M + H]^{+1}$	1.376	151.9
622.028960	$P_3N_3(OCH_3CF_2)_6[M + H]^{+1}$	1.013	202.4
922.009798	$P_3N_3(OCH_3CF_2CF_2)_6[M + H]^{+1}$	0.835	243.8
1221.990637	$P_3N_3(OCH_3C_2F_4CF_2)_6[M + H]^{+1}$	0.740	274.1
1521.971475	$P_3N_3(OCH_3C_3F_6CF_2)_6[M + H]^{+1}$	0.638	317.2
1821.952313	$P_3N_3(OCH_3C_4F_8CF_2)_6[M + H]^{+1}$	0.590	342.5
2121.933152	$P_3N_3(OCH_3C_5F_{10}CF_2)_6[M + H]^{+1}$	0.520	388.3
2421.913992	$P_3N_3(OCH_3C_6F_{12}CF_2)_6[M + H]^{+1}$	0.469	429.5
2721.894829	$P_3N_3(OCH_3C_7F_{14}CF_2)_6[M + H]^{+1}$	0.444	447.4
301.998139	$C_3N_3(CF_3)_3[M]^{-1}$	1.909	109.6
601.978977	$C_3N_3((CF_2)_2CF_3)_3[M]^{-1}$	1.187	172.8
1033.988109	$P_3N_3(OCH_3CF_2CF_2)_6[M + C_2F_3O_2]^{-1}$	0.776	261.9
1333.968947	$P_3N_3(OCH_3C_2F_4CF_2)_6[M + C_2F_3O_2]^{-1}$	0.710	285.4
1633.949786	$P_3N_3(OCH_3C_3F_6CF_2)_6[M + C_2F_3O_2]^{-1}$	0.609	332.1
1933.930624	$P_3N_3(OCH_3C_4F_8CF_2)_6[M + C_2F_3O_2]^{-1}$	0.573	352.5
2233.911463	$P_3N_3(OCH_3C_5F_{10}CF_2)_6[M + C_2F_3O_2]^{-1}$	0.498	405.2
2533.892301	$P_3N_3(OCH_3C_6F_{12}CF_2)_6[M + C_2F_3O_2]^{-1}$	0.465	433.6
2833.873139	$P_3N_3(OCH_3C_7F_{14}CF_2)_6[M + C_2F_3O_2]^{-1}$	0.399	505.1

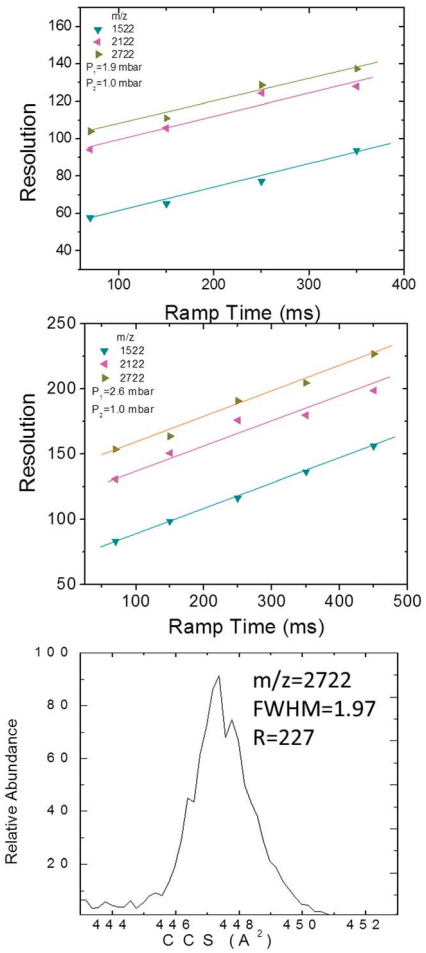

Fig. 8 (Top) Mobility resolution as a function of the ramp time for the sphere-like ESI Tuning Mix standards for $P_1 = 1.9$ and 2.6 mbar and $P_2 = 1.0$ mbar, respectively. (Bottom) IMS profile for $m/z = 2722$ with RF = 300 V_{pp}, $T_{ramp} = 450$ ms and $P_1 = 2.6$ and $P_2 = 1.0$ mbar.

counteract the increased drag force of the ions. The latter results in an increase in the mobility resolution (see Fig. 8). In the case of the ramp speed, the narrower the ΔV_{ramp} and the larger the T_{ramp} the higher the mobility resolution; that is, the slower the scan speed the higher the mobility resolution for a given bath gas velocity (see Fig. 8). For the conditions explored in the present work, mobility resolution values of 100–250 were routinely obtained. It should be noted that the ramp time can be increased for up to a few seconds in a TIMS device with small to no ion loss (current limitations are on the electronic acquisition of long IMS transients). For the case of RF confinement, as discussed before, the lower the RF needed to confine the ions the smaller the axial spread for the same number of ions in the ion cloud (see the example in the ESI†). It should be noted that the number of ions can also be varied using the source conditions and the duration of the fill injection pulse, thus allowing for the highest resolution possible.

Conclusions

Ion dynamics simulations showed the ion dynamics inside of a trapped ion mobility spectrometer as a function of the bath gas velocity and trapping conditions. Simulations showed the effect of the radial confinement on the ion cloud, which ultimately translates into the mobility resolution of the analyser. It was shown that the main parameters that define the ion motion in a TIMS analyser are the drift gas velocity, the ion confinement and the electric field ramp speed. Comparison of theoretical and experimental values results that the parabolic gas velocity profile can increase the axial spread of the trapped ions; however, the radial confinement counteracts the axial spread by confining the ions to the central region of the TIMS analyzer where a more homogenous gas speed is obtained. Experimental results showed that mobility values can be extracted using first principles, analogous to drift tube designs; the main difference is that internal or external calibration standards are needed for accurate measurements of mobility values for each experimental condition (*e.g.*, velocity of the gas and voltage ramp). Results are shown for high mobility resolution (R = 100–250) over a wide mobility range.

Notes and references

1 P. Dwivedi, P. Wu, S. Klopsch, G. Puzon, L. Xun and H. Hill, Metabolic profiling by ion mobility mass spectrometry (IMMS), *Metabolomics*, 2008, **4**, 63–80.
2 R. Fernandez-Maestre, C. S. Harden, R. G. Ewing, C. L. Crawford and H. H. Hill, Chemical standards in ion mobility spectrometry, *Analyst*, 2010, **135**, 1433–1442.
3 G. A. Eiceman, E. V. Krylov, N. S. Krylova, E. G. Nazarov and R. A. Miller, Separation of Ions from Explosives in Differential Mobility Spectrometry by Vapor-Modified Drift Gas, *Anal. Chem.*, 2004, **76**, 4937–4944.
4 E. V. Krylov, S. L. Coy, J. Vandermey, B. B. Schneider, T. R. Covey and E. G. Nazarov, Selection and generation of waveforms for differential mobility spectrometry, *Rev. Sci. Instrum.*, 2010, **81**, 024101.
5 W. Cheung, Y. Xu, C. L. Thomas and R. Goodacre, Discrimination of bacteria using pyrolysis-gas chromatography-differential mobility spectrometry (Py-GC-DMS) and chemometrics, *Analyst*, 2009, **134**, 557–563.
6 T. Koimtzis, N. J. Goddard, I. Wilson and C. L. Thomas, Assessment of the feasibility of the use of conductive polymers in the fabrication of ion mobility spectrometers, *Anal. Chem.*, 2011, **83**, 2613–2621.
7 V. Moll, V. Bocos-Bintintan, I. A. Ratiu, D. Ruszkiewicz and C. L. Thomas, Control of dopants/modifiers in differential mobility spectrometry using a piezoelectric injector, *Analyst*, 2012, **137**, 1458–1465.
8 W. Vautz, R. Slodzynski, C. Hariharan, L. Seifert, J. Nolte, R. Fobbe, S. Sielemann, B. C. Lao, R. Huo, C. L. Thomas and L. Hildebrand, Detection of metabolites of trapped humans using ion mobility spectrometry coupled with gas chromatography, *Anal. Chem.*, 2013, **85**, 2135–2142.
9 S. Prasad, H. Schmidt, P. Lampen, M. Wang, R. Guth, J. V. Rao, G. B. Smith and G. A. Eiceman, Analysis of bacterial strains with pyrolysis-gas chromatography/differential mobility spectrometry, *Analyst*, 2006, **131**, 1216–1225.

10 P. R. Kemper and M. T. Bowers, A hybrid double-focusing mass spectrometer-high-pressure drift reaction cell to study thermal energy reactions of mass-selected ions, *J. Am. Soc. Mass Spectrom.*, 1990, **1**, 197–207.
11 C. Wu, W. F. Siems, G. R. Asbury and H. H. Hill, Electrospray Ionization High-Resolution Ion Mobility Spectrometry-Mass Spectrometry, *Anal. Chem.*, 1998, **70**, 4929–4938.
12 Y. Liu and D. E. Clemmer, Characterizing Oligosaccharides Using Injected-Ion Mobility/Mass Spectrometry, *Anal. Chem.*, 1997, **69**, 2504–2509.
13 M. F. Jarrold and V. A. Constant, Silicon cluster ions: Evidence for a structural transition, *Phys. Rev. Lett.*, 1991, **67**, 2994.
14 F. A. Fernandez-Lima, R. C. Blase and D. H. Russell, A study of ion-neutral collision cross-section values for low charge states of peptides, proteins, and peptide/protein complexes, *Int. J. Mass Spectrom.*, 2010, **298**, 111–118.
15 F. A. Fernandez-Lima, H. Wei, Y. Q. Gao and D. H. Russell, On the Structure Elucidation Using Ion Mobility Spectrometry and Molecular Dynamics, *J. Phys. Chem. A*, 2009, **113**, 8221–8234.
16 F. A. Fernandez-Lima, C. Becker, A. M. McKenna, R. P. Rodgers, A. G. Marshall and D. H. Russell, Petroleum Crude Oil Characterization by IMS-MS and FTICR MS, *Anal. Chem.*, 2009, **81**, 9941–9947.
17 F. A. Fernandez-Lima, C. Becker, K. J. Gillig, W. K. Russell, S. E. Tichy and D. H. Russell, Ion Mobility-Mass Spectrometer Interface for Collisional Activation of Mobility Separated Ions, *Anal. Chem.*, 2009, **81**, 618–624.
18 C. Becker, F. A. Fernández-Lima, K. J. Gillig, W. K. Russell, S. Cologna and D. H. Russell, A Novel Collision-Induced Dissociation (CID) Experiment for Ion Mobility-Mass Spectrometry, *J. Am. Soc. Mass Spectrom.*, 2009, **20**, 907–914.
19 F. A. Fernandez-Lima, C. Becker, K. Gillig, W. K. Russell, M. A. C. Nascimento and D. H. Russell, Experimental and Theoretical Studies of (CsI)nCs+ Cluster Ions Produced by 355 nm Laser Desorption Ionization, *J. Phys. Chem. A*, 2008, **112**, 11061–11066.
20 A. B. Kanu, P. Dwivedi, M. Tam, L. Matz and H. H. Hill, Ion mobility-mass spectrometry, *J. Mass Spectrom.*, 2008, **43**, 1–22.
21 S. L. Koeniger, S. I. Merenbloom, S. J. Valentine, M. F. Jarrold, H. R. Udseth, R. D. Smith and D. E. Clemmer, An IMS-IMS Analogue of MS-MS, *Anal. Chem.*, 2006, **78**, 4161–4174.
22 K. J. Gillig and D. H. Russell, A periodic field focusing ion mobility spectrometer, *US Pat.*, The Texas A & M University System, *United States*, 2001, vol. WO0165589, p. 36.
23 K. J. Gillig, B. T. Ruotolo, E. G. Stone and D. H. Russell, An electrostatic focusing ion guide for ion mobility-mass spectrometry, *Int. J. Mass Spectrom.*, 2004, **239**, 43–49.
24 B. M. Kolakowski and Z. Mester, Review of applications of high-field asymmetric waveform ion mobility spectrometry (FAIMS) and differential mobility spectrometry (DMS), *Analyst*, 2007, **132**, 842–864.
25 E. G. Nazarov, R. A. Miller, G. A. Eiceman and J. A. Stone, Miniature differential mobility spectrometry using atmospheric pressure photoionization, *Anal. Chem.*, 2006, **78**, 4553–4563.
26 Y. Guo, J. Wang, G. Javahery, B. A. Thomson and K. W. M. Siu, Ion Mobility Spectrometer with Radial Collisional Focusing, *Anal. Chem.*, 2004, **77**, 266–275.
27 R. S. Glaskin, M. A. Ewing and D. E. Clemmer, Ion Trapping for Ion Mobility Spectrometry Measurements in a Cyclical Drift Tube, *Anal. Chem.*, 2013, **85**, 7003–7008.
28 S. D. Pringle, K. Giles, J. L. Wildgoose, J. P. Williams, S. E. Slade, K. Thalassinos, R. H. Bateman, M. T. Bowers and J. H. Scrivens, An investigation of the mobility separation of some peptide and protein ions using a new hybrid quadrupole/travelling wave IMS/oa-ToF instrument, *Int. J. Mass Spectrom.*, 2007, **261**, 1–12.
29 P. Dugourd, R. R. Hudgins, D. E. Clemmer and M. F. Jarrold, High-resolution ion mobility measurements, *Rev. Sci. Instrum.*, 1997, **68**, 1122–1129.
30 S. I. Merenbloom, R. S. Glaskin, Z. B. Henson and D. E. Clemmer, High-Resolution Ion Cyclotron Mobility Spectrometry, *Anal. Chem.*, 2009, **81**, 1482–1487.
31 P. R. Kemper, N. F. Dupuis and M. T. Bowers, A new, higher resolution, ion mobility mass spectrometer, *Int. J. Mass Spectrom.*, 2009, **287**, 46–57.
32 R. C. Blase, J. A. Silveira, K. J. Gillig, C. M. Gamage and D. H. Russell, Increased ion transmission in IMS: A high resolution, periodic-focusing DC ion guide ion mobility spectrometer, *Int. J. Mass Spectrom.*, 2011, **301**, 166–173.
33 F. A. Fernandez-Lima, D. A. Kaplan and M. A. Park, Gas-phase separation using a trapped ion mobility spectrometer, *Int. J. Ion Mobility Spectrom.*, 2011, **14**, 93–98.
34 F. A. Fernandez-Lima, D. A. Kaplan and M. A. Park, Integration of trapped ion mobility spectrometry with mass spectrometry, *Rev. Sci. Instrum.*, 2011, **82**, 126106.
35 P. H. Dawson, *Quadrupole Mass Sprectrometry and Its Applications*, AIP Press, Woodbury, NY, 1995.
36 L. A. Viehland and E. A. Mason, Gaseous ion mobility and diffusion in electric fields of arbitrary strength, *Ann. Phys.*, 1978, **110**, 287–328.
37 B. T. Ruotolo, J. A. McLean, K. J. Gillig and D. H. Russell, The influence and utility of varying field strength for the separation of tryptic peptides by ion mobility-mass spectrometry, *J. Am. Soc. Mass Spectrom.*, 2005, **16**, 158–165.
38 L. A. Flanagan, Mass Spectrometry calibration using homogeneously substituted fluorinated triazatriphosphorines, *US Pat.*, Hewlett-Packard Company, Palo Alto, CA, United States, 1999, vol. 5872357, p. 19.
39 CFD Fluent, *Fluent 6.2.16*, Fluent Inc., Lebanon, NH.
40 *Simion 3D*, Scientific Instrument Services, Inc., Ringoes, NJ.
41 L. Ding, M. Sudakov and S. Kumashiro, A simulation study of the digital ion trap mass spectrometer, *Int. J. Mass Spectrom.*, 2002, **221**, 117–138.
42 C. Henry, Product Review: Building A Better Trap, *Anal. Chem.*, 1998, **70**, 533A–536A.
43 K. J. Gillig, B. K. Bluhm and D. H. Russell, Ion motion in a Fourier transform ion cyclotron resonance wire ion guide

cell, *Int. J. Mass Spectrom. Ion Processes*, 1996, **157–158**, 129–147.

44 E. N. Nikolaev, R. M. Heeren, A. M. Popov, A. V. Pozdneev and K. S. Chingin, Realistic modeling of ion cloud motion in a Fourier transform ion cyclotron resonance cell by use of a particle-in-cell approach, *Rapid Commun. Mass Spectrom.*, 2007, **21**, 3527–3546.

45 S. Kim, M. C. Choi, S. Kim, M. Hur, H. S. Kim, J. S. Yoo, G. T. Blakney, C. L. Hendrickson and A. G. Marshall, Modification of Trapping Potential by Inverted Sidekick Electrode Voltage During Detection To Extend Time-Domain Signal Duration for Significantly Enhanced Fourier Transform Ion Cyclotron Resonance Mass Resolution, *Anal. Chem.*, 2007, **79**, 3575–3580.

46 T. M. Schaub, C. L. Hendrickson, S. Horning, J. P. Quinn, M. W. Senko and A. G. Marshall, High-Performance Mass Spectrometry: Fourier Transform Ion Cyclotron Resonance at 14.5 Tesla, *Anal. Chem.*, 2008, **80**, 3985–3990.

47 J. Zeleny, On the ratio of velocities of the two ions produced in gases by Röngten radiation, and on some related phenomena, *Philos. Mag.*, 1898, **46**, 120–154.

48 M. A. Park, Apparatus and method for parallel flow ion mobility spectrometry combined with mass spectrometry, *US Pat.*, Bruker Daltonics, Inc., Billerica, MA, United States, 2010, vol. 7838826.

49 E. W. McDaniel and E. A. Mason, *Mobility and diffusion of ions in gases*, John Wiley and Sons, Inc., New York, 1973.

50 L. A. Viehland and E. A. Mason, Gaseous ion mobility in electric fields of arbitrary strength, *Ann. Phys.*, 1975, **91**, 499–533.

51 P. Watts and A. Wilders, On the resolution obtainable in practical ion mobility systems, *Int. J. Mass Spectrom. Ion Processes*, 1992, **112**, 179–190.

52 G. F. Verbeck, B. T. Ruotolo, K. J. Gillig and D. H. Russell, Resolution equations for high-field ion mobility, *J. Am. Soc. Mass Spectrom.*, 2004, **15**, 1320–1324.